Relativistic many-body calculations of energies for core-excited states in sodiumlike ions

U. I. Safronova,* W. R. Johnson,† and M. S. Safronova‡
Department of Physics, 225 Nieuwland Science Hall, University of Notre Dame, Notre Dame, Indiana 46566

J. R. Albritton
Lawrence Livermore National Laboratory, P.O. Box 808, Livermore, California 94551

(Received 17 June 2002; revised manuscript received 5 August 2002; published 17 October 2002)

Energies of $2s^22p^53l3l'$ and $2s2p^63l3l'$ states for sodiumlike ions with $Z=14-100$ are evaluated to second order in relativistic many-body perturbation theory starting from a neonlike Dirac-Fock potential. Second-order Coulomb and Breit interactions are included. Correction for the frequency dependence of the Breit interaction is taken into account in the lowest order. The Lamb shift correction to energies is also included in the lowest order. Intrinsic particle-particle-hole contributions to energies are found to be 20–30 % of the sum of one- and two-body contributions. Comparisons are made with available experimental data. These calculations are presented as a theoretical benchmark for comparison with experiment and theory.

DOI: 10.1103/PhysRevA.66.042506 PACS number(s): 31.15.Ar, 31.15.Md, 31.25.Jf, 32.30.Rj

I. INTRODUCTION

Core-excited states of Na-like ions have two valence electrons outside and one hole inside a closed $n=2$ core and, therefore, present an excellent model for studying strong correlations in systems with closely spaced levels. We carry out second-order relativistic many-body perturbation theory (RMBPT) calculations for Na-like ions starting from a $1s^22s^22p^6$ Dirac-Fock (DF) potential. All possible $2l$ holes and $3l'3l''$ particles leading to 121 odd-parity and 116 even-parity $3l'3l''[J_1]2l^{-1}(J)$ states are considered. We calculate energies of the 237 core-excited states together with the $3l$ singly excited states in Na-like ions with nuclear charges Z ranging from 14 to 100.

Many experimental values for the energy levels and fine-structure intervals are now available up to very high nuclear charge ($Z=57$) for $3l'3l''[J_1]2l^{-1}(J)$ levels; additionally, experimental rates for some transitions between these levels are available. The objective of this paper is to present a comprehensive set of calculations for $3l'3l''[J_1]2l^{-1}(J)$ energies to compare with previous calculations and experiments for the entire Na isoelectronic sequence. Most of earlier measurements and calculations focused on the $3s^2[^1S]2p^{-1}\ ^2P_J$ states and low-lying $3s3p[^3P]2p^{-1}\ ^4D_J$ and $3s3d[^3D]2p^{-1}\ ^4F_J$ levels. Very few results exist for other $3p^22p^{-1}$, $3s3p2p^{-1}$, and $3s3d2p^{-1}$ levels. The large number of possible transitions have made experimental identification difficult. Experimental verification should become simpler and more reliable using this more accurate and complete set of calculations.

We start with a brief overview of previous theoretical and experimental studies of properties of core-excited states in sodiumlike ions. Energies, collision strengths, and oscillator strengths for $2s^22p^63l$-$2s^22p^53l'3l''$ and $2s^22p^63l$-$2s2p^63l'3l''$ transitions in Na-like ions with nuclear charges $22\leqslant Z\leqslant 62$ were calculated by Zhang *et al.* [1], where energies and mixing coefficients were obtained using the Cowan code [2] with a scaling factor $(Z-3.9)/Z$. In the paper by Chen [3], Auger and radiative transition energies and rates were calculated for 18 ions with nuclear charges in the range $18\leqslant Z\leqslant 92$ using the multiconfiguration Dirac-Fock method. Wavelengths, radiative transition rates, Auger rates, satellite intensity factors, and fluorescence yields were presented by Nilsen [4] for dielectronic satellites of 14 neonlike ions (Ar^{8+}-W^{64+}) including $2s^22p^63l$-$2s^22p^53l'3l''$ and $2s^22p^63l$-$2s2p^63l'3l''$ transitions. The calculations in Ref. [4] were made using the YODA code that is based on multiconfiguration relativistic functions for the bound states and distorted-wave Dirac wave functions for continuum electrons. New comprehensive theoretical analyses of the $2s^22p^53lnl'$ and $2s2p^63lnl'$ ($n=3-8$) doubly excited states in Fe^{15+} and Cu^{18+} were presented by Bruch *et al.* [5,6]. In these papers, energy levels, radiative transitions probabilities, and autoionization rates were calculated by using the Cowan and YODA codes. Recently, *R*-matrix calculations of electron-impact collision strengths for excitation from the inner L shell into doubly excited states of Fe^{15+} were presented by Bautista [7]. Energy positions of the $2s^22p^63l$ and $2s^22p^53l3l'$ states were calculated in that work using the SUPERSTRUCTURE code of Eissner *et al.* [8]. It was shown in Ref. [7] that disagreement between calculations and data recommended by Sugar and Corliss [9] and Shirai *et al.* [10] ranges from 0.5% to 5%.

Studies of the $2s^22p^53lnl'$ configurations in Na-like ions are of continuing interest from both theoretical and experimental points of view. Experimentally, these configurations are studied by photon and electron emission spectroscopy. To our knowledge, the first measurements of $2p$-$3s$ and $2p$-$3d$ transitions in Na-like Fe (which included the $2s^22p^53l3l'$ configurations) using photon emission spectroscopy were done by Burkhalter *et al.* [11] in 1979. The soft x-ray spectra produced by a focused laser source and a vacuum spark device were obtained in Ref. [11] using a grazing incidence

*Electronic address: usafrono@nd.edu
†Electronic address: johnson@nd.edu
‡Present address: Electron and Optical Physics Division, National Institute of Standards and Technology, Gaithersburg, MD 20899-8410.

 ©2002 The American Physical Society

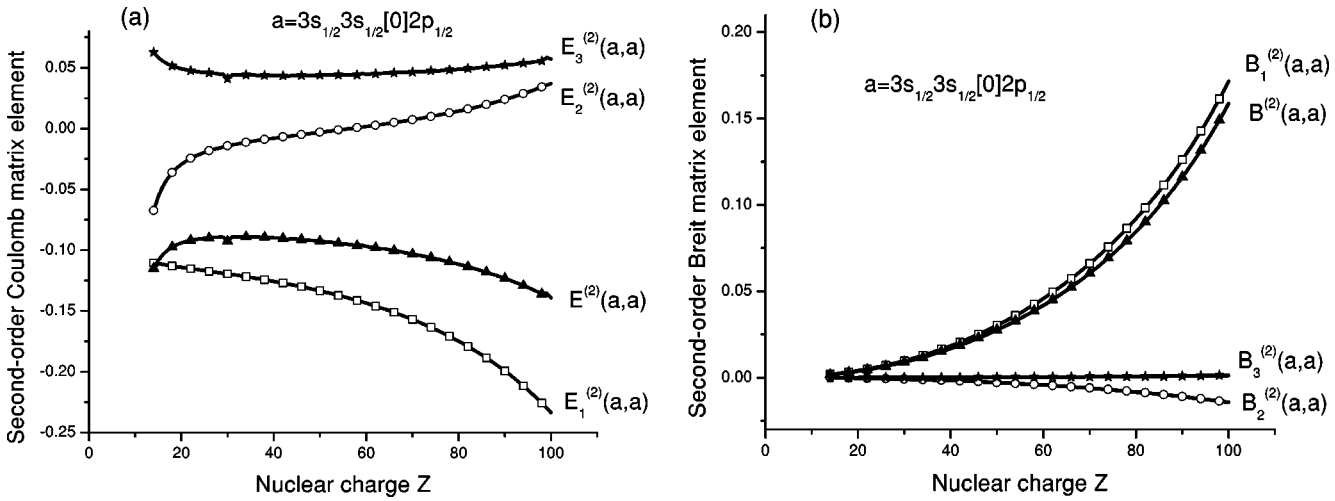

FIG. 1. Second-order Coulomb (a) and Breit (b) energy contributions to diagonal matrix elements in Na-like ions.

spectrograph. Identification of the spectra was based on theoretical calculations using the Cowan code. The $2s^2 2p^5 3s 3p\ ^4D_{7/2}$-$2s^2 2p^5 3s 3d\ ^4G_{9/2}$ transition in Fe XVI was observed by the beam-foil technique by Jupén *et al.* [12]. The identification of this transition was based on a study of the difference in wave numbers between experimental values and theoretical predictions obtained from the Cowan code in Na-like ions from S VI to Cu XIX. Auger electron spectra of Na-like Fe ions excited in collisions of 170-keV Fe XVIII on He and Ne were studied by Schneider *et al.* [13]. The dominant spectral structures were due to Auger decay of states with $2s^2 2p^5 3l 3l'$ configurations in Fe XVI. Special attention was paid to the metastable level $2s^2 2p^5 3s 3p\ ^4D_{7/2}$ which was studied in detail; the absolute energy of this level was measured. Three of the 17 lines observed in this experiment were identified with states from $2s^2 2p^5 3l 4l'$ configurations. This analysis was based on theoretical predictions using the multiconfigurational Dirac-Fock method including the transverse Breit interaction. A few years later this analysis was extended to include an isoelectronic study of double electron capture in slow ion-atom collisions of F-like ions (Si^{5+}, Ar^{9+}, Sc^{12+}, Ti^{13+}, Fe^{17+}, and Cu^{20+}) with He atoms [14]. It was reported that the metastable level $2s^2 2p^5 3s 3p\ ^4D_{7/2}$ was observed in all Auger spectra except Si^{3+}. Recently in Ref. [15], a study of the double electron capture in low-energy Fe^{17+} + He collisions was conducted. Except for the confirmation of the identification of the 12 peaks in the 225–340 eV interval, predictions were made for identification of four additional peaks in the 585–670 eV interval. A comparison of solar and tokamak Fe XVII x-ray spectra with synthetic spectra including dielectronic satellites with $2s^2 2p^6 nl$-$2s^2 2p^5 3snl$ and $2s^2 2p^6 nl$-$2s^2 2p^5 3dnl$ transitions was presented by Phillips *et al.* [16]. Atomic data were calculated by Phillips *et al.* [16] using the SUPERSTRUCTURE code. Recently, the three Fe^{15+} inner-shell satellite lines were thoroughly studied at the Lawrence Livermore National Laboratory electron beam ion trap EBIT-II by Brown *et al.* [17].

In the present paper, we use RMBPT to determine energies of $2s^2 2p^5 3l 3l'$ and $2s 2p^6 3l 3l'$ states for Na-like ions

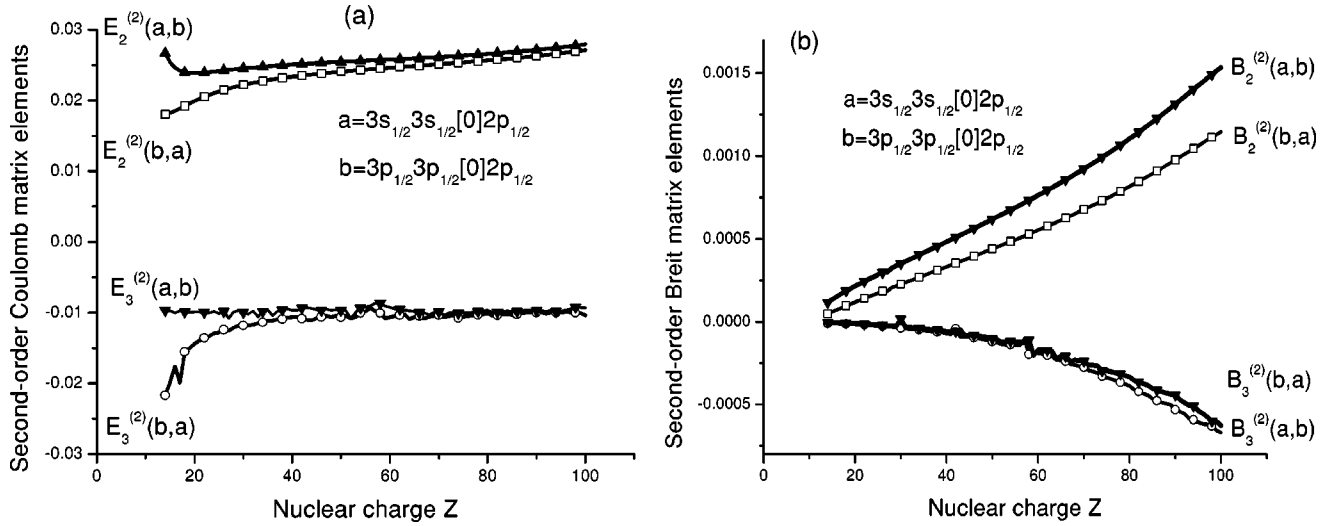

FIG. 2. Second-order Coulomb (a) and Breit (b) energy contributions to nondiagonal matrix elements in Na-like ions.

TABLE I. Second-order contributions to the energy matrices (a.u.) for odd-parity states with $J=1/2$ in the case of Na-like iron, $Z=26$. One-body, two-body, and three-body second-order Coulomb contributions are given in columns labeled $E_1^{(2)}$, $E_2^{(2)}$, and $E_3^{(2)}$, respectively.

$3l_1j_13l_2j_2[J_1]2l_3j_3$	$3l_1j_13l_2j_2[J_1]2l_3j_3$	$E_1^{(2)}$	$E_2^{(2)}$	$E_3^{(2)}$	$B_1^{(2)}$	$B_2^{(2)}$	$B_3^{(2)}$
$3s_{1/2}3s_{1/2}[0]2p_{1/2}$	$3s_{1/2}3s_{1/2}[0]2p_{1/2}$	−0.117383	−0.018247	0.045731	0.007176	−0.000575	0.000038
$3s_{1/2}3d_{3/2}[1]2p_{3/2}$	$3s_{1/2}3d_{3/2}[1]2p_{3/2}$	−0.120539	−0.044013	0.063988	0.007397	−0.000260	0.000023
$3p_{1/2}3p_{3/2}[1]2p_{3/2}$	$3p_{1/2}3p_{3/2}[1]2p_{3/2}$	−0.121263	−0.028980	0.047458	0.006851	−0.001224	0.000078
$3p_{1/2}3p_{3/2}[2]2p_{3/2}$	$3p_{1/2}3p_{3/2}[2]2p_{3/2}$	−0.121263	−0.049640	0.047326	0.006851	−0.001303	−0.000066
$3p_{3/2}3p_{3/2}[2]2p_{3/2}$	$3p_{3/2}3p_{3/2}[2]2p_{3/2}$	−0.120687	−0.029376	0.056161	0.006774	−0.000707	0.000057
$3p_{1/2}3p_{1/2}[0]2p_{1/2}$	$3p_{1/2}3p_{1/2}[0]2p_{1/2}$	−0.125451	−0.036306	0.055166	0.006661	−0.001531	0.000080
$3s_{1/2}3s_{1/2}[0]2p_{1/2}$	$3p_{1/2}3p_{1/2}[0]2p_{1/2}$	0.000000	0.024260	−0.009791	0.000000	0.000298	−0.000020
$3p_{1/2}3p_{1/2}[0]2p_{1/2}$	$3s_{1/2}2s_{1/2}[0]2p_{1/2}$	0.000000	0.021498	−0.012387	0.000000	0.000184	−0.000026

with nuclear charges in the range of $Z=14-100$. Our calculations are carried out to second order in perturbation theory and include second-order Coulomb and Breit interactions. Corrections for the frequency-dependent Breit interaction are taken into account in the lowest order. Screened self-energy and vacuum polarization data given by Blundell [18] are used to determine the QED correction.

Our perturbation theory calculations are carried out using single-particle orbitals calculated in the DF potential of the Ne-like core. As a first step, we determine and store the single-particle contributions to the energies for three $n=2$ hole states ($2s$, $2p_{1/2}$, and $2p_{3/2}$) and the five $n=3$ valence states ($3s$, $3p_{1/2}$, $3p_{3/2}$, $3d_{3/2}$, and $3d_{5/2}$) in lowest, first, and second orders. Next, we evaluate and store the 155 two-particle $\langle 3l3l'\ J|H^{\rm eff}|3l''3l'''\ J\rangle$ matrix elements and the 178 hole-particle $\langle 2l3l'\ J|H^{\rm eff}|2l''3l'''\ J\rangle$ matrix elements of the effective Hamiltonian in the first and second orders. It should be noted that these one-particle, two-particle, and hole-particle matrix elements were used previously to evaluate energies of the $3l3l'$ levels in Mg-like ions [19] and energies of the $2l^{-1}3l'$ levels in neonlike ions [20]. Finally, second-order particle-particle-hole matrix elements are evaluated. Combining these data using the method described below, we calculate one-, two-, and three-body contributions to the energies of Na-like ions.

The present calculations are compared with experimental and predicted results from Refs. [12,15,21,22].

II. METHOD

The RMBPT formalism developed previously [23–25] for B-like and Al-like ions is used here to describe the perturbed wave functions and to obtain the second-order energies [23] of the core-excited states of Na-like ions. The particle-particle-hole contribution to the energies of those states is, however, different from the three-particle contribution to the energies of B-like and Al-like ions, and is derived in the appendix. Including hole-particle matrix elements in Na-like ions leads to 237 $3l3l'2l^{-1}$ states instead of 148 $3l3l'3l''$ states of Al-like ions or 15 $2l2l'2l''$ of B-like ions and, consequently, to more laborious numerical calculations.

A. Model space

The model space for core-excited $3l3l'2l^{-1}$ states of Na-like ions includes 121 odd-parity states consisting of 25 $J=1/2$ states, 37 $J=3/2$ states, 31 $J=5/2$ states, 19 $J=7/2$

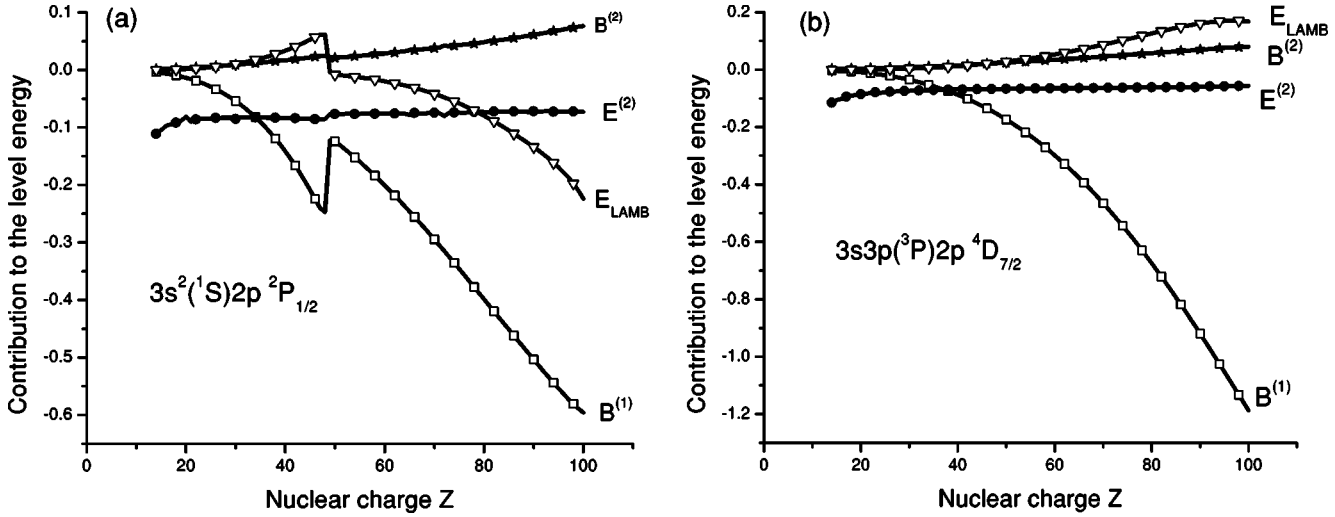

FIG. 3. Contributions to the energies of the $3s^2(^1S)2p\ ^2P_{1/2}$ (a) and $3s3p(^3P)2p\ ^4D_{7/2}$ (b) levels of Na-like ions.

TABLE II. Energies of odd-parity levels with $J=1/2$ of Na-like iron, $Z=26$ in a.u. $E^{(0+1)}\equiv E^{(0)}+E^{(1)}+B^{(1)}$.

LS coupling	$E^{(0+1)}$	$E^{(2)}$	$B^{(2)}$	E_{LAMB}	E_{tot}	*jj* coupling
$3s3s(^1S)2p\ ^2P$	8.773110	−0.083480	0.006746	0.005992	8.702368	$3s_{1/2}3s_{1/2}[0]2p_{1/2}$
$3p3p(^1D)2p\ ^2P$	10.670626	−0.077625	0.006239	−0.000404	10.598835	$3s_{1/2}3d_{3/2}[1]2p_{3/2}$
$3p3p(^3P)2p\ ^4P$	10.835054	−0.086763	0.006247	−0.000386	10.754151	$3p_{1/2}3p_{3/2}[1]2p_{3/2}$
$3p3p(^3P)2p\ ^4D$	11.078592	−0.094598	0.005974	−0.000075	10.989892	$3p_{1/2}3p_{3/2}[2]2p_{3/2}$
$3s3d(^3D)2p\ ^4P$	11.124410	−0.093485	0.007247	0.001962	11.040134	$3p_{3/2}3p_{3/2}[2]2p_{3/2}$
$3p3p(^3P)2p\ ^2S$	11.250339	−0.092918	0.006029	0.000379	11.163829	$3p_{1/2}3p_{1/2}[0]2p_{1/2}$

states, 7 $J=9/2$ states, and two $J=11/2$ states. Additionally, there are 116 even-parity states consisting of 25 $J=1/2$ states, 35 $J=3/2$ states, 31 $J=5/2$ states, 17 $J=7/2$ states, 7 $J=9/2$ states, and one $J=11/2$ state.

The evaluation of the second-order energies for the $3l3l'[J_1]2l^{-1}(J)$ states in Na-like ions follows the pattern of the corresponding calculation for Mg-like and Ne-like ions given in Refs. [19,20]. In particular, we use the second-order one-particle and two-particle matrix elements for Mg-like ions calculated in Ref. [19] and hole-particle matrix elements for Ne-like ions calculated in Ref. [20]. These matrix elements are recoupled as described below to obtain the one-body and two-body contributions for Na-like ions. We will discuss how these matrix elements are combined to obtain the one-body and two-body contributions to energies of Na-like ions. We refer the reader to Refs. [19], [20] for a discussion of the evaluation of the one-body and two-body matrix elements. An intrinsic particle-particle-hole diagram also contributes to the second-order energy for Na-like ions. The expression for the particle-particle-hole diagram differs from the expression for the three-particle diagram given in Ref. [23] owing to different angular parts. The expression for the intrinsic particle-particle-hole diagram is derived in the appendix.

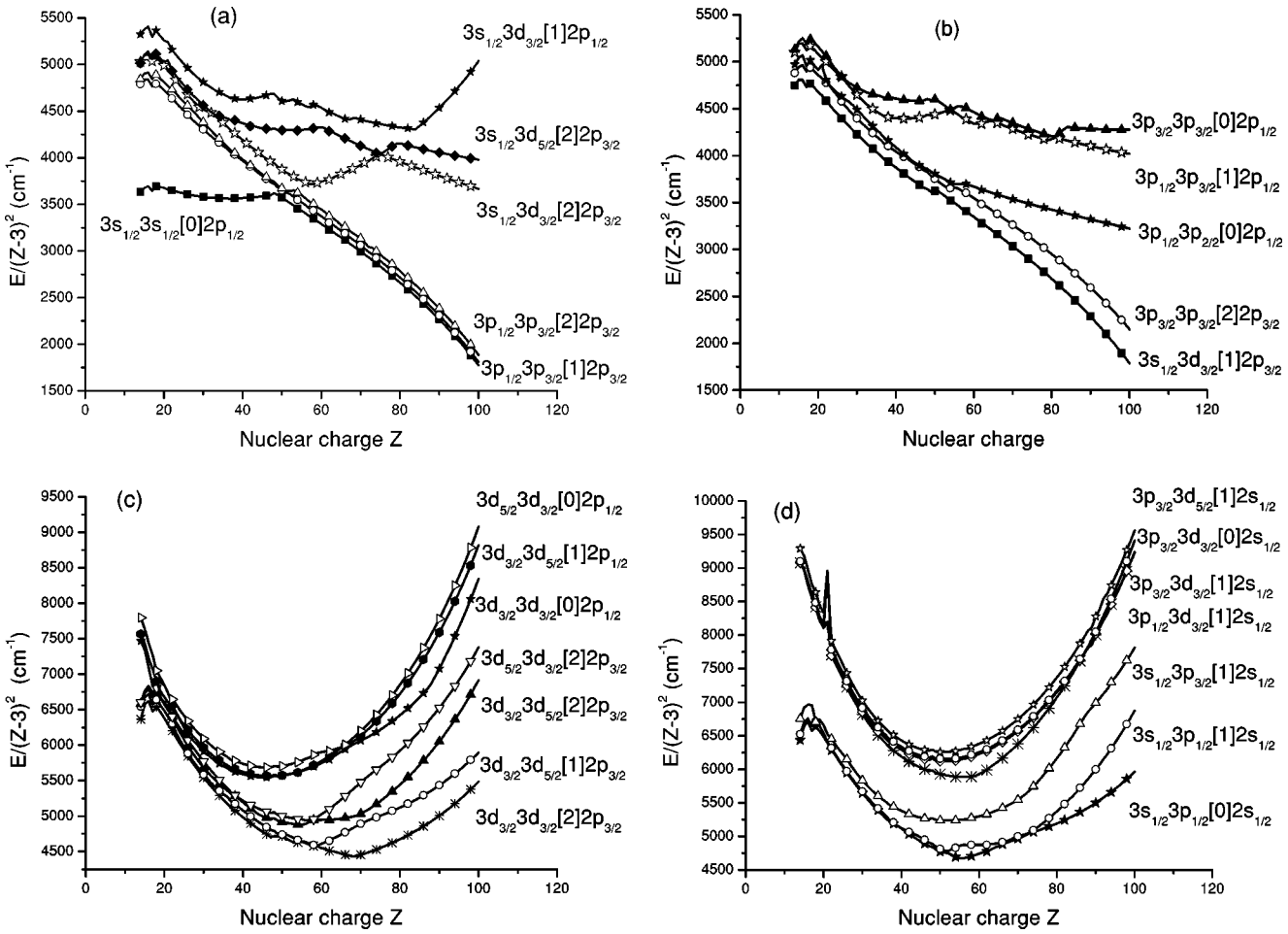

FIG. 4. Energies $[E/(Z-3)^2$ in $\mathrm{cm}^{-1}]$ of odd-parity states with $J=1/2$ as functions of Z.

TABLE III. Energies of Na-like ions relative to the ground state of Ne-like ions in cm^{-1} for ions with $Z=26-57$.

LS scheme	$Z=26$	$Z=29$	$Z=32$	$Z=36$	$Z=42$	$Z=47$	$Z=54$	$Z=57$	*jj* scheme
$3s\ ^2S_{1/2}$	−3946654	−5408870	−7101306	−9720897	−14444875	−19131372	−26886482	−30654172	$3s_{1/2}$
$3s3s(^1S)2p\ ^2P_{3/2}$	1808945	2258991	2745096	3441058	4560251	5526519	6849732	7377220	$3s_{1/2}3s_{1/2}[0]2p_{3/2}$
$3s3s(^1S)2p\ ^2P_{1/2}$	1909949	2425440	3005011	3882164	5436825	6970009	9000854	9844722	$3s_{1/2}3s_{1/2}[0]2p_{1/2}$
$3s3p(^3P)2p\ ^4S_{3/2}$	2008738	2500357	3029307	3783964	4993448	6037431	7475330	8054553	$3s_{1/2}3p_{1/2}[0]2p_{3/2}$
$3s3p(^3P)2p\ ^4D_{5/2}$	2033074	2527745	3060001	3820060	5040067	6094393	7547744	8133682	$3s_{1/2}3p_{1/2}[1]2p_{3/2}$
$3s3p(^3P)2p\ ^4D_{7/2}$	2039466	2544056	3092521	3887772	5202696	6391332	8153954	8929008	$3s_{1/2}3p_{3/2}[2]2p_{3/2}$
$3s3p(^3P)2p\ ^4D_{3/2}$	2039528	2535211	3068422	3830075	5053095	6110756	7569587	8158101	$3s_{1/2}3p_{1/2}[1]2p_{3/2}$
$3s3p(^1P)2p\ ^2P_{1/2}$	2050246	2548295	3083346	3846505	5069726	6126870	7585055	8173589	$3s_{1/2}3p_{1/2}[1]2p_{3/2}$
$3s3p(^1P)2p\ ^2D_{3/2}$	2064245	2571269	3121744	3919367	5237983	6430207	8198752	8976653	$3s_{1/2}3p_{3/2}[1]2p_{3/2}$
$3s3p(^3P)2p\ ^4P_{5/2}$	2064483	2573798	3127096	3928976	5254252	6451971	8228075	9009218	$3s_{1/2}3p_{3/2}[1]2p_{3/2}$
$3s3p(^1P)2p\ ^2S_{1/2}$	2081011	2593540	3150111	3956604	5289060	6493231	8278916	9064324	$3s_{1/2}3p_{3/2}[1]2p_{3/2}$
$3s3p(^3P)2p\ ^4D_{1/2}$	2129621	2676539	3264927	4098156	5504613	6756597	8605934	9416474	$3s_{1/2}3p_{3/2}[2]2p_{3/2}$
$3s3p(^3P)2p\ ^4P_{1/2}$	2135848	2685223	3305872	4239177	5881367	7491636	9880164	10785869	$3s_{1/2}3p_{1/2}[0]2p_{1/2}$
$3s3p(^3P)2p\ ^4D_{3/2}$	2140088	2685129	3252230	4070053	5417213	6632701	8434674	9227490	$3s_{1/2}3p_{3/2}[2]2p_{3/2}$
$3s3p(^3P)2p\ ^2D_{5/2}$	2148356	2668661	3231730	4045552	5387153	6598225	8393917	9183909	$3s_{1/2}3p_{3/2}[2]2p_{3/2}$
$3s3p(^3P)2p\ ^4P_{3/2}$	2151490	2701237	3326210	4266154	5921839	7543576	9927031	10836191	$3s_{1/2}3p_{1/2}[1]2p_{1/2}$
$3s3p(^1P)2p\ ^2D_{5/2}$	2160829	2733488	3378432	4358921	6115991	7878203	9971617	10881891	$3s_{1/2}3p_{3/2}[2]2p_{1/2}$
$3s3p(^1P)2p\ ^2P_{3/2}$	2165759	2724616	3366873	4344602	6098245	7861912	10139433	11066015	$3s_{1/2}3p_{3/2}[1]2p_{1/2}$
$3s3p(^3P)2p\ ^2P_{1/2}$	2234248	2803037	3437436	4387010	6072516	7718801	10074749	10996341	$3s_{1/2}3p_{1/2}[1]2p_{1/2}$
$3s3p(^3P)2p\ ^2D_{3/2}$	2253626	2839597	3496708	4490270	6270868	7858384	10205550	11168436	$3s_{1/2}3p_{3/2}[2]2p_{1/2}$
$3s3p(^3P)2p\ ^2S_{1/2}$	2299453	2882506	3533957	4517384	6280342	7824403	10160693	11394844	$3s_{1/2}3p_{3/2}[1]2p_{1/2}$
$3p3p(^3P)2p\ ^4P_{3/2}$	2323992	2875690	3466402	4305185	5644107	6799972	8402456	9055318	$3p_{1/2}3p_{1/2}[0]2p_{3/2}$
$3s3d(^1D)2p\ ^2P_{1/2}$	2326176	2884880	3488911	4360343	5793880	7086329	9174130	10022351	$3s_{1/2}3d_{3/2}[1]2p_{3/2}$
$3p3p(^3P)2p\ ^4P_{5/2}$	2331859	2890891	3494970	4366156	5799124	7090560	9005390	9849121	$3p_{1/2}3p_{3/2}[1]2p_{3/2}$
$3p3p(^1D)2p\ ^2F_{7/2}$	2340430	2900161	3504745	4375109	5807350	7097923	9010959	9853573	$3p_{1/2}3p_{3/2}[2]2p_{3/2}$
$3p3p(^3P)2p\ ^4P_{3/2}$	2343264	2903098	3506655	4376509	5807902	7098885	9013658	9857413	$3p_{1/2}3p_{3/2}[1]2p_{3/2}$
$3p3p(^3P)2p\ ^4P_{1/2}$	2360263	2934357	3558208	4462832	5937498	7244558	9239436	10097513	$3p_{1/2}3p_{3/2}[1]2p_{3/2}$
$3p3p(^3P)2p\ ^2D_{3/2}$	2360688	2923345	3530947	4407111	5848142	7146773	9072189	9920622	$3p_{1/2}3p_{3/2}[2]2p_{3/2}$
$3p3p(^1D)2p\ ^2D_{5/2}$	2361387	2925210	3533627	4410325	5851442	7149759	9074248	9921995	$3p_{1/2}3p_{3/2}[2]2p_{3/2}$
$3p3p(^3P)2p\ ^4D_{7/2}$	2366738	2941047	3566519	4478642	5996208	7322997	9275443	10133874	$3p_{3/2}3p_{3/2}[2]2p_{3/2}$
$3p3p(^3P)2p\ ^4D_{5/2}$	2367125	2941219	3566447	4478544	6004427	7321838	9262357	10114485	$3p_{3/2}3p_{3/2}[2]2p_{3/2}$
$3p3p(^3P)2p\ ^4D_{1/2}$	2412003	2993290	3608811	4494602	5959608	7285858	9436271	10311330	$3p_{1/2}3p_{3/2}[2]2p_{3/2}$
$3p3p(^3P)2p\ ^4S_{3/2}$	2419891	3004313	3622761	4511681	5970412	7282549	9224215	10078225	$3p_{3/2}3p_{3/2}[2]2p_{3/2}$
$3s3d(^3D)2p\ ^4P_{1/2}$	2423029	2998759	3630191	4541409	6064401	7447505	9514794	10579279	$3p_{3/2}3p_{3/2}[2]2p_{3/2}$
$3s3d(^3D)2p\ ^4P_{3/2}$	2432332	3009247	3646026	4568623	6048355	7371746	9328624	10189264	$3p_{3/2}3p_{3/2}[0]2p_{3/2}$
$3s3d(^3D)2p\ ^4F_{9/2}$	2441515	3018138	3640285	4537586	6017419	7358627	9367047	10262012	$3s_{1/2}3d_{5/2}[3]2p_{3/2}$
$3p3p(^3P)2p\ ^4D_{3/2}$	2442028	3044141	3676510	4576282	6090589	7459516	9498136	10404492	$3s_{1/2}3d_{3/2}[1]2p_{3/2}$
$3s3d(^3D)2p\ ^4P_{5/2}$	2444121	3022154	3645035	4540867	6009260	7354901	9320567	10184749	$3s_{1/2}3d_{3/2}[1]2p_{3/2}$
$3p3p(^1D)2p\ ^2F_{5/2}$	2446690	3035904	3658924	4555153	6029241	7401210	9431150	10330672	$3s_{1/2}3d_{3/2}[2]2p_{3/2}$
$3s3d(^3D)2p\ ^4F_{7/2}$	2448304	3025385	3646951	4541206	6018858	7410665	9465885	10368561	$3s_{1/2}3d_{3/2}[2]2p_{3/2}$
$3p3p(^3P)2p\ ^2S_{1/2}$	2450177	3066099	3702033	4615334	6110247	7495342	9669557	10796904	$3p_{1/2}3p_{1/2}[0]2p_{1/2}$
$3s3d(^3D)2p\ ^4F_{5/2}$	2457171	3059907	3688115	4592423	6082264	7445653	9536164	10459319	$3s_{1/2}3d_{5/2}[2]2p_{3/2}$
$3p3p(^1S)2p\ ^2P_{3/2}$	2458536	3050488	3688938	4624648	6178953	7590274	9666579	10585200	$3s_{1/2}3d_{3/2}[2]2p_{3/2}$
$3s3d(^3D)2p\ ^4F_{3/2}$	2467888	3072651	3726831	4658307	6214029	7658925	9924797	10978300	$3s_{1/2}3d_{5/2}[2]2p_{3/2}$
$3s3d(^3D)2p\ ^4D_{7/2}$	2473728	3057201	3686257	4592770	6086770	7440067	9484093	10396064	$3s_{1/2}3d_{5/2}[2]2p_{3/2}$
$3p3p(^1D)2p\ ^2D_{3/2}$	2474319	3087038	3769447	4742709	6305020	7764437	10055141	11119321	$3s_{1/2}3d_{5/2}[3]2p_{3/2}$
$3s3d(^1D)2p\ ^2P_{1/2}$	2475520	3073042	3769007	4724883	6270683	7669065	9823175	10854112	$3s_{1/2}3d_{3/2}[2]2p_{3/2}$
$3s3d(^1D)2p\ ^2F_{5/2}$	2476256	3072416	3770426	4716884	6243639	7642346	9827384	10855818	$3s_{1/2}3d_{5/2}[3]2p_{3/2}$
$3p3p(^3P)2p\ ^2D_{5/2}$	2478055	3117666	3792216	4823275	6692492	8552527	11702449	12906145	$3p_{1/2}3p_{3/2}[2]2p_{1/2}$
$3s3d(^3D)2p\ ^2P_{3/2}$	2494618	3110698	3801760	4822655	6690006	8549142	11693655	12876722	$3p_{1/2}3p_{3/2}[1]2p_{1/2}$
$3s3d(^3D)2p\ ^4D_{1/2}$	2503765	3111834	3774944	4819276	6600142	8335220	11178869	12561626	$3s_{1/2}3d_{5/2}[2]2p_{3/2}$
$3s3d(^3D)2p\ ^4D_{3/2}$	2532307	3146832	3830007	4918354	6841218	8727106	11696997	13061250	$3p_{1/2}3p_{3/2}[2]2p_{1/2}$
$3s3d(^3D)2p\ ^2F_{7/2}$	2536607	3128717	3766505	4684639	6205225	7605894	9808688	10842983	$3s_{1/2}3d_{5/2}[3]2p_{3/2}$

TABLE III. (*Continued*).

LS scheme	$Z=26$	$Z=29$	$Z=32$	$Z=36$	$Z=42$	$Z=47$	$Z=54$	$Z=57$	*jj* scheme
$3s3d(^3D)2p\ ^4D_{5/2}$	2553254	3150273	3837776	4932054	6886124	8784045	11721257	13062930	$3p_{3/2}3p_{3/2}[2]2p_{1/2}$
$3s3d(^3D)2p\ ^4F_{3/2}$	2553625	3193957	3905127	4973425	6875056	8755816	11862792	13125630	$3p_{3/2}3p_{3/2}[2]2p_{1/2}$
$3s3d(^1D)2p\ ^2D_{5/2}$	2554863	3199650	3916483	4994914	6912385	8834753	11836413	13135682	$3s_{1/2}3d_{3/2}[2]2p_{1/2}$
$3p3p(^1S)2p\ ^2P_{1/2}$	2560337	3171081	3838660	4841463	6685037	8542196	11682890	12867258	$3p_{1/2}3p_{3/2}[1]2p_{1/2}$

B. Energy-matrix elements

In Fig. 1(a) we present the one-body, $E_1^{(2)}(a,a)$, two-body, $E_2^{(2)}(a,a)$, and three-body, $E_3^{(2)}(a,a)$ Coulomb contributions to the diagonal matrix element with $a=3s_{1/2}3s_{1/2}[0]2p_{1/2}(1/2)$ as functions of Z. Here and in the sequel, we drop the superscript -1 on the $n=2$ hole state for simplicity. We see from Fig. 1(a) that the value of $E_3^{(2)}(a,a)$ is almost constant for all Z. The one-body contribution is the largest one. The sum of $E_2^{(2)}(a,a)$ and $E_3^{(2)}(a,a)$ values is almost equal to zero for small-Z ions; however, the three-body contribution becomes more important with increasing Z. As a result, the total second-order Coulomb contribution $E^{(2)}(a,a)=E_1^{(2)}(a,a)+E_2^{(2)}(a,a)+E_3^{(2)}(a,a)$ differs from the one-body contribution and is almost constant for all Z. In Fig. 1(b), we present the one-body, $B_1^{(2)}(a,a)$, two-body, $B_2^{(2)}(a,a)$, and three-body, $B_3^{(2)}\times(a,a)$ Breit-Coulomb contributions to the diagonal matrix element with $a=3s_{1/2}3s_{1/2}[0]2p_{1/2}(1/2)$ as functions of Z. The one-body contribution is the largest among other contributions and the total Breit second-order contribution $B^{(2)}\times(a,a)=B_1^{(2)}(a,a)+B_2^{(2)}(a,a)+B_3^{(2)}(a,a)$ is almost equal to the one-body contribution. The one-body contribution vanishes for nondiagonal matrix elements.

In Fig. 2(a), we illustrate the contributions $E_2^{(2)}$ and $E_3^{(2)}$ for two nondiagonal elements $E_i^{(2)}(a,b)$ and $E_i^{(2)}(b,a)$ with $a=3s_{1/2}3s_{1/2}[0]2p_{1/2}(1/2)$ and $b=3p_{1/2}3p_{1/2}[0]2p_{1/2}(1/2)$. The corresponding Breit contributions are plotted in Fig. 2(b). We see from Fig. 2(a) that the ratio of $E_3^{(2)}$ to $E_2^{(2)}$ is about 30–50 % for high-Z ions. Figure 2(a) illustrates the asymmetry of the nondiagonal energy matrix elements for low-Z ions. The asymmetry of the two-particle second-order matrix elements in RMBPT calculation was discussed in Ref. [26]. Values of $E_2^{(2)}$ and $E_3^{(2)}$ have different signs and the total second-order contribution $E^{(2)}$ is about half of $E_2^{(2)}$. The behavior of nondiagonal second-order Breit contribution is shown in Fig. 2(b). The $B_2^{(2)}$ and $B_3^{(2)}$ increase with Z; however, they have opposite signs. The total second-order contribution $B^{(2)}$ can be about half of $B_2^{(2)}$. Finally, we observe some small deviations from smooth Z dependences of $E_3^{(2)}$ and $B_3^{(2)}$ in Figs. 2(a) and 2(b). As we can see from Eq. (A10) in the appendix, the denominator $\varepsilon(v)+\varepsilon(w)-\varepsilon(a)-\varepsilon(n)$ in the expression for the three-body diagram contains two valence energies $\varepsilon(v)$, $\varepsilon(w)$, one hole energy $\varepsilon(a)$, and one virtual-state energy $\varepsilon(n)$. The sum $\varepsilon(3s)+\varepsilon(3s)-\varepsilon(2p)$ is positive; therefore, the denominator can be close to zero when $\varepsilon(n)$ is positive. In such a case, a singularity arises from the contribution of the continuous part of spectra to the sum over states for the $E_3^{(2)}$ and $B_3^{(2)}$ matrix elements, resulting in sharp features in the corresponding Z dependences.

Numerical values of the contributions to second-order energies are given for the special case of Na-like iron, $Z=26$, in Table I. We list one-body, two-body, and three-body second-order Coulomb and Breit contributions to the energy matrices, labeled $E_i^{(2)}$ and $B_i^{(2)}$, $i=1,2,3$, respectively. The one-body second-order energies are obtained as sums of the two valence and one hole energies; therefore, the values of $E_1^{(2)}$ are nonzero only for diagonal matrix elements.

C. Eigenvalues and eigenvectors for core-excited states

After evaluating the energy matrices, we calculate eigenvalues and eigenvectors for states with given values of J and parity. There are two possible methods to carry out the diagonalization: (a) diagonalize the sum of zeroth- and first-order matrices, then calculate the second-order contributions using the resulting eigenvectors or (b) diagonalize the sum of the zeroth-, first-, and second-order matrices together. Following Ref. [23], we choose the second method here.

The importance of second-order contributions to the energies is illustrated in Fig. 3. In this figure, the second-order energy $E^{(2)}$, the first- and second-order Breit contributions $B^{(1)}$ and $B^{(2)}$, and the QED contribution E_{LAMB} are plotted as functions of nuclear charge Z for the $3s^2(^1S)2p\ ^2P_{1/2}$ (a) and $3s3p(^3P)2p\ ^4D_{7/2}$ (b) states of Na-like ions. We can see from the figure that $E^{(2)}$ dominates up to $Z=34$ and $Z=37$ for the $3s^22p\ ^2P_{1/2}$ and $3s3p(^3P)2p\ ^4D_{7/2}$ states, respectively. The QED contribution E_{LAMB} is smaller than the $E^{(2)}$ energy up to $Z=50$ for the energy level shown in Fig. 3(a) and $Z=60$ for the energy level shown in Fig. 3(b). The second-order Breit energy $B^{(2)}$ is smaller than the second-order energy $E^{(2)}$ up to $Z=97$ [Fig. 3(a)] and $Z=83$ [Fig. 3(b)], respectively.

As a specific example, we list in Table II the following contributions to the energies of six excited states in Fe^{15+}: $E^{(0+1)}=E^{(0)}+E^{(1)}+B^{(1)}$, the second-order Coulomb and Breit contributions $E^{(2)}$ and $B^{(2)}$, the QED correction E_{LAMB}, and the total theoretical energy E_{tot}. The QED correction is approximated as the sum of the one-electron self-energy and the first-order vacuum-polarization energy. The screened self-energy and vacuum-polarization data given by Blundell [18] are used to determine the QED correction E_{LAMB} (see Ref. [19] for detail).

TABLE IV. Auger energies in Fe^{15+} in eV. Comparison with predicted data (E_{fit}) from Bliman *et al.* [15].

LS scheme	E_{RMBPT}	E_{fit}	*jj* scheme	*LS* scheme	E_{RMBPT}	E_{fit}	*jj* scheme
$3s3s(^1S)2p\ ^2P_{3/2}$	224.3	225.0	$3s_{1/2}3s_{1/2}[0]2p_{3/2}$	$3p3p(^3P)2p\ ^4D_{5/2}$	293.5	293.6	$3p_{3/2}3p_{3/2}[2]2p_{3/2}$
$3s3s(^1S)2p\ ^2P_{1/2}$	236.8	237.3	$3s_{1/2}3s_{1/2}[0]2p_{1/2}$	$3p3p(^3P)2p\ ^4D_{1/2}$	299.1		$3p_{1/2}3p_{3/2}[2]2p_{3/2}$
$3s3p(^3P)2p\ ^4S_{3/2}$	249.1	249.5	$3s_{1/2}3p_{1/2}[0]2p_{3/2}$	$3p3p(^3P)2p\ ^4S_{3/2}$	300.0	300.4	$3p_{3/2}3p_{3/2}[2]2p_{3/2}$
$3s3p(^3P)2p\ ^4D_{5/2}$	252.1	252.4	$3s_{1/2}3p_{1/2}[1]2p_{3/2}$	$3s3d(^3D)2p\ ^4P_{1/2}$	300.4		$3p_{3/2}3p_{3/2}[2]2p_{3/2}$
$3s3p(^3P)2p\ ^4D_{7/2}$	252.9	253.2	$3s_{1/2}3p_{3/2}[2]2p_{3/2}$	$3s3d(^3D)2p\ ^4P_{3/2}$	301.6		$3p_{3/2}3p_{3/2}[0]2p_{3/2}$
$3s3p(^3P)2p\ ^4D_{3/2}$	252.9	253.2	$3s_{1/2}3p_{1/2}[1]2p_{3/2}$	$3s3d(^3D)2p\ ^4F_{9/2}$	302.7	303.6	$3s_{1/2}3d_{5/2}[3]2p_{3/2}$
$3s3p(^1P)2p\ ^2P_{1/2}$	254.2	254.6	$3s_{1/2}3p_{1/2}[1]2p_{3/2}$	$3p3p(^3P)2p\ ^4D_{3/2}$	302.8		$3s_{1/2}3d_{3/2}[1]2p_{3/2}$
$3s3p(^1P)2p\ ^2D_{3/2}$	255.9	256.0	$3s_{1/2}3p_{3/2}[1]2p_{3/2}$	$3s3d(^3D)2p\ ^4P_{5/2}$	303.0	303.7	$3s_{1/2}3d_{3/2}[1]2p_{3/2}$
$3s3p(^3P)2p\ ^4P_{5/2}$	256.0	256.1	$3s_{1/2}3p_{3/2}[1]2p_{3/2}$	$3p3p(^1D)2p\ ^2F_{5/2}$	303.4		$3s_{1/2}3d_{3/2}[2]2p_{3/2}$
$3s3p(^1P)2p\ ^2S_{1/2}$	258.0	258.3	$3s_{1/2}3p_{3/2}[1]2p_{3/2}$	$3s3d(^3D)2p\ ^4F_{7/2}$	303.6	304.4	$3s_{1/2}3d_{3/2}[2]2p_{3/2}$
$3s3p(^3P)2p\ ^4D_{1/2}$	264.0	264.5	$3s_{1/2}3p_{3/2}[2]2p_{3/2}$	$3p3p(^3P)2p\ ^2S_{1/2}$	303.8		$3p_{1/2}3p_{1/2}[0]2p_{1/2}$
$3s3p(^3P)2p\ ^4P_{1/2}$	264.8	265.1	$3s_{1/2}3p_{1/2}[0]2p_{1/2}$	$3s3d(^3D)2p\ ^4F_{5/2}$	304.7	305.3	$3s_{1/2}3d_{5/2}[2]2p_{3/2}$
$3s3p(^3P)2p\ ^4D_{3/2}$	265.3	265.7	$3s_{1/2}3p_{3/2}[2]2p_{3/2}$	$3p3p(^1S)2p\ ^2P_{3/2}$	304.8		$3s_{1/2}3d_{3/2}[2]2p_{3/2}$
$3s3p(^3P)2p\ ^2D_{5/2}$	266.4	266.5	$3s_{1/2}3p_{3/2}[2]2p_{3/2}$	$3s3d(^3D)2p\ ^4F_{3/2}$	306.0		$3s_{1/2}3d_{5/2}[2]2p_{3/2}$
$3s3p(^3P)2p\ ^4P_{3/2}$	266.8	267.1	$3s_{1/2}3p_{1/2}[1]2p_{1/2}$	$3s3d(^3D)2p\ ^4D_{7/2}$	306.7		$3s_{1/2}3d_{5/2}[2]2p_{3/2}$
$3s3p(^1P)2p\ ^2D_{5/2}$	267.9	268.1	$3s_{1/2}3p_{3/2}[2]2p_{1/2}$	$3p3p(^1D)2p\ ^2D_{3/2}$	306.8		$3s_{1/2}3d_{5/2}[3]2p_{3/2}$
$3s3p(^1P)2p\ ^2P_{3/2}$	268.5	268.5	$3s_{1/2}3p_{3/2}[1]2p_{1/2}$	$3s3d(^1D)2p\ ^2P_{1/2}$	306.9		$3s_{1/2}3d_{3/2}[2]2p_{3/2}$
$3s3p(^3P)2p\ ^2P_{1/2}$	277.0	277.1	$3s_{1/2}3p_{1/2}[1]2p_{1/2}$	$3s3d(^1D)2p\ ^2F_{5/2}$	307.0		$3s_{1/2}3d_{5/2}[3]2p_{3/2}$
$3s3p(^3P)2p\ ^2D_{3/2}$	279.4	279.6	$3s_{1/2}3p_{3/2}[2]2p_{1/2}$	$3p3p(^3P)2p\ ^2D_{5/2}$	307.2		$3p_{1/2}3p_{3/2}[2]2p_{1/2}$
$3s3p(^3P)2p\ ^2S_{1/2}$	285.1	285.1	$3s_{1/2}3p_{3/2}[1]2p_{1/2}$	$3s3d(^3D)2p\ ^2P_{3/2}$	309.3		$3p_{1/2}3p_{3/2}[1]2p_{1/2}$
$3p3p(^3P)2p\ ^4P_{3/2}$	288.1	289.2	$3p_{1/2}3p_{1/2}[0]2p_{3/2}$	$3s3d(^3D)2p\ ^4D_{1/2}$	310.4		$3s_{1/2}3d_{5/2}[2]2p_{3/2}$
$3s3d(^1D)2p\ ^2P_{1/2}$	288.4	289.6	$3s_{1/2}3d_{3/2}[1]2p_{3/2}$	$3s3d(^3D)2p\ ^4D_{3/2}$	314.0		$3p_{1/2}3p_{3/2}[2]2p_{1/2}$
$3p3p(^3P)2p\ ^4P_{5/2}$	289.1	290.0	$3p_{1/2}3p_{3/2}[1]2p_{3/2}$	$3s3d(^3D)2p\ ^2F_{7/2}$	314.5		$3s_{1/2}3d_{5/2}[3]2p_{3/2}$
$3p3p(^1D)2p\ ^2F_{7/2}$	290.2	291.3	$3p_{1/2}3p_{3/2}[2]2p_{3/2}$	$3s3d(^3D)2p\ ^4D_{5/2}$	316.6		$3p_{3/2}3p_{3/2}[2]2p_{1/2}$
$3p3p(^3P)2p\ ^4P_{3/2}$	290.5		$3p_{1/2}3p_{3/2}[1]2p_{3/2}$	$3s3d(^3D)2p\ ^4F_{3/2}$	316.6	317.1	$3p_{3/2}3p_{3/2}[2]2p_{1/2}$
$3p3p(^3P)2p\ ^4P_{1/2}$	292.6		$3p_{1/2}3p_{3/2}[1]2p_{3/2}$	$3s3d(^1D)2p\ ^2D_{5/2}$	316.8		$3s_{1/2}3d_{3/2}[2]2p_{1/2}$
$3p3p(^3P)2p\ ^2D_{3/2}$	292.7	293.3	$3p_{1/2}3p_{3/2}[2]2p_{3/2}$	$3p3p(^1S)2p\ ^2P_{1/2}$	317.4		$3p_{1/2}3p_{3/2}[1]2p_{1/2}$
$3p3p(^1D)2p\ ^2D_{5/2}$	292.8		$3p_{1/2}3p_{3/2}[2]2p_{3/2}$	$3p3p(^3P)2p\ ^2P_{1/2}$	317.5		$3p_{3/2}3p_{3/2}[0]2p_{1/2}$
$3p3p(^3P)2p\ ^4D_{7/2}$	293.4	294.1	$3p_{3/2}3p_{3/2}[2]2p_{3/2}$				

The sharp features in the curves shown in Fig. 3(a) are explained by strong mixing of states inside of the odd-parity complex with $J=1/2$. The main contribution to the $3s^2(^1S)2p\ ^2P_{1/2}$ level comes from the $3s_{1/2}3s_{1/2}[0]2p_{1/2}$ state for ions with small Z up to $Z=48$. Starting from $Z=49$, the main contribution to this level comes from the $3p_{1/2}3p_{3/2}[1]2p_{3/2}$ and $3p_{1/2}3p_{3/2}[2]2p_{3/2}$ states instead of the $3s_{1/2}3s_{1/2}[0]2p_{1/2}$ state.

The particle-particle-hole levels studied in this work may be divided to two groups by their energies: those with energies in the range of 15–23 a.u and those with energies greater than 25 a.u. The first group of levels includes the $3s_{1/2}3s_{1/2}[0]2p_j$, $3s_{1/2}3d_j[J_1]2p_{j'}$, $3p_j3p_{j'}[J_1]2p_{j''}$, and $3s_{1/2}3p_j[J_1]2p_{j'}$ levels (64 levels total). The second group includes the remaining 173 levels. The first group of levels has been studied experimentally, while there are no experimental data for the second group.

When starting calculations from relativistic DF wave functions, it is natural to use *jj* designations for uncoupled energy matrix elements; however, neither *jj* nor *LS* coupling describes *physical* states properly, except for the single-configuration state $3p_{3/2}3d_{5/2}[4]2p_{3/2} \equiv 3p3d(^3F)2p\ ^3G_{11/2}$. Both designations are given in our subsequent tables.

The Z dependence of the eigenvalues of the $3lj3l'j'[J_1]2l''j''(J)$ odd-parity states with $J=1/2$ is given in Figs. 4(a)–(d), where the energies are divided by $(Z-3)^2$. Scaled energies $E/(Z-3)^2$ decrease with Z for the first group of levels [Figs. 4(a) and 4(b)] and have parabolic Z dependence for the second group [Figs. 4(c) and 4(d)]. It is evident from Figs. 4(a) and 4(b) that there is a strong mixing between the $3s_{1/2}3s_{1/2}[0]2p_{1/2}$, $3s_{1/2}3d_j[J_1]2p_{j'}$, and $3p_j3p_{j'}[J_1]2p_{j''}$ levels. We already mentioned that a strong mixing occurs between the $3s_{1/2}3s_{1/2}[0]2p_{3/2}$, $3p_{1/2}3p_{3/2}[1]2p_{3/2}$, and $3p_{1/2}3p_{3/2}[2]2p_{3/2}$ states for $Z=48-49$.

It should be noted that the *LS* designations are chosen by comparing results with available experimental data for low-Z ions. We used the labeling of levels from Refs. [5], [6], where the identification of levels in Fe^{15+} and Cu^{18+} was based on the Cowan code. We already mentioned that there are no measurements for the second group of levels, therefore, we do not give *LS* designations for the levels shown in Figs. 4(c) and 4(d). The change of the relative magnitude of mixing coefficients is illustrated by the behavior of the six levels in Fig. 4(a) and the five levels in Fig. 4(b). The crossing of levels inside a complex (set of levels with the same J and parity) is forbidden by the Wigner-Neumann theorem [27].

TABLE V. Wavelengths λ in angstroms for Na-like ions for odd-parity states given relative to the ground state. Comparison with experimental results from Ref. [21] (λ_a) and Ref. [22] (λ_b).

Configuration	J	$Z=47$		$Z=57$	
		λ_{RMBPT}	λ_a	λ_{RMBPT}	λ_b
$3s_{1/2}3s_{1/2}[0]2p_{3/2}$	1.5	4.0555	4.0547	2.6294	2.6294
$3s_{1/2}3s_{1/2}[0]2p_{1/2}$	0.5	3.8312	3.8309	2.4692	
$3s_{1/2}3d_{3/2}[2]2p_{3/2}$	1.5	3.7423	3.7427	2.4249	
$3s_{1/2}3d_{5/2}[2]2p_{1/2}$	2.5	3.5707	3.571	2.2788	
$3p_{3/2}p_{3/2}[0]2p_{1/2}$	0.5	3.5701	3.571	2.2798	
$3s_{1/2}3d_{3/2}[2]2p_{1/2}$	1.5	3.5700	3.571	2.2766	
$3s_{1/2}3p_{3/2}[1]2s_{1/2}$	1.5	3.4261	3.426	2.1805	
$3s_{1/2}3p_{3/2}[1]2s_{1/2}$	0.5	3.4121	3.412	2.1739	

III. COMPARISON OF RESULTS WITH OTHER THEORIES AND EXPERIMENTS

We have calculated energies of the 121 odd-parity states and the 116 even-parity excited states for Na-like ions with nuclear charges ranging from $Z=14$ to 100. In Table III, we illustrate our theoretical results giving energies of the 38 odd-parity states $3s^2(^1S)2p\ ^2P_J$, $3s3d(^{1,3}D)2p\ ^{2,4}L_J$, and $3p^2(^{1,3}L')2p\ ^{2,4}L_J$ and the 18 even-parity states $3s3p(^{1,3}P)2p\ ^{2,4}L_J$ for eight Na-like ions with nuclear charges ranging from $Z=26$ to $Z=57$. We also include the ground state $3s\ ^2S_{1/2}$ energies in the table.

A. Excitation energies

Comparisons of our RMBPT energies with other theoretical and experimental data are too voluminous to include here; therefore, we present several examples of comparisons for selected levels and ions. In Table IV, our theoretical results for $3s^2(^1S)2p\ ^2P_J$, $3s3p(^{1,3}P)2p\ ^{2,4}L_J$, $3p^2(^{1,3}L')2p\ ^{2,4}L_J$, and $3s3d(^{1,3}D)2p\ ^{2,4}L_J$ levels of Na-like Fe are compared with predicted Auger energies given by Bliman *et al.* [15]. It should be noted that the predicted Auger energies in Ref. [15] differ by 1 eV from experimental measurements presented more than 15 years ago by Schneider *et al.* [13], where the method of zero-degree Auger spectroscopy was used to study the excitation and decay of Auger states formed in 170-keV Fe^{17+} ions with He and Ne target atoms. Our RMBPT energies are in much better agreement with recent results from Ref. [15] than with experimental measurements from Ref. [13].

TABLE VI. Wavelengths λ in angstroms for the $3s3p(^3P)2p\ ^4D_{7/2}-3s3d(^3D)2p\ ^4F_{9/2}$ transition in Na-like ions with $Z=15-30$. Comparison with experimental (λ_{expt}) and predicted (λ_{fit}) data from Jupen *et al.* [12].

Z	λ_{RMBPT}	λ_{expt}	λ_{fit}
15	729.74		728.3
16	613.99	614.06±0.08	614.20
17	534.12	532.70±0.10	532.67
18	472.79	471.34±0.05	471.22
19	424.23		424.05
20	384.80		384.15
21	350.86		351.98
22	325.76	324.87±0.02	324.89
23	302.61		301.69
24	281.75	281.67±0.08	281.60
25	264.32		263.98
26	248.73	248.36±0.05	248.39
27	234.76		234.48
28	222.26	222.00±0.10	221.98
29	210.93	210.70±0.05	210.68
30	200.63		200.39

In Table V, our RMBPT wavelengths for Na-like Ag and La are compared with experimental results presented by Beiersdorfer *et al.* [21,22]. Spectra of the $n=3$ to $n=2$ transitions in neonlike silver obtained from the Princeton Large Torus (PLT) were recorded with a high-resolution Bragg-crystal spectrometer. The measurements covered the wavelength interval 3.3-4.1 Å. Eight lines of Na-like Ag were observed. As one can see from Table V, our theoretical calculations are in excellent agreement with results from Ref. [21]. Measurement of a single line in Na-like La was carried out with a high-resolution crystal spectrometer on the PLT tokamak by Beiersdorfer *et al.* [22]. Our RMBPT result agrees with experimental wavelengths from Ref. [22] to five significant figures. We list our theoretical data for other lines in La^{46+} in Table V.

The $3s3p(^3P)2p\ ^4D_{7/2}$-$3s3d(^3D)2p\ ^4F_{9/2}$ transitions in P^{4+}-Zn^{19+} ions were investigated by Jupén *et al.* [12]. Identification of spectral lines originating from the transitions between core-excited configurations in Na isoelectronic sequence was made from analyses of beam-foil spectra in Ref. [12]. Wavelengths λ_{expt} from Ref. [12] are shown in Table VI together with our RMBPT data λ_{RMBPT}. We also present the predicted data λ_{fit} from Ref. [12] in the same table. The predicted wavelengths were obtained in Ref. [12] from the fit of the difference between experimental data and Cowan code calculations. Our *ab initio* calculations are in good agreement with those predictions.

B. Fine structure of the ^2L and ^4L terms in core-excited states of Na-like ions

No measurements of fine-structure intervals were made by observing the wavelength differences between transitions

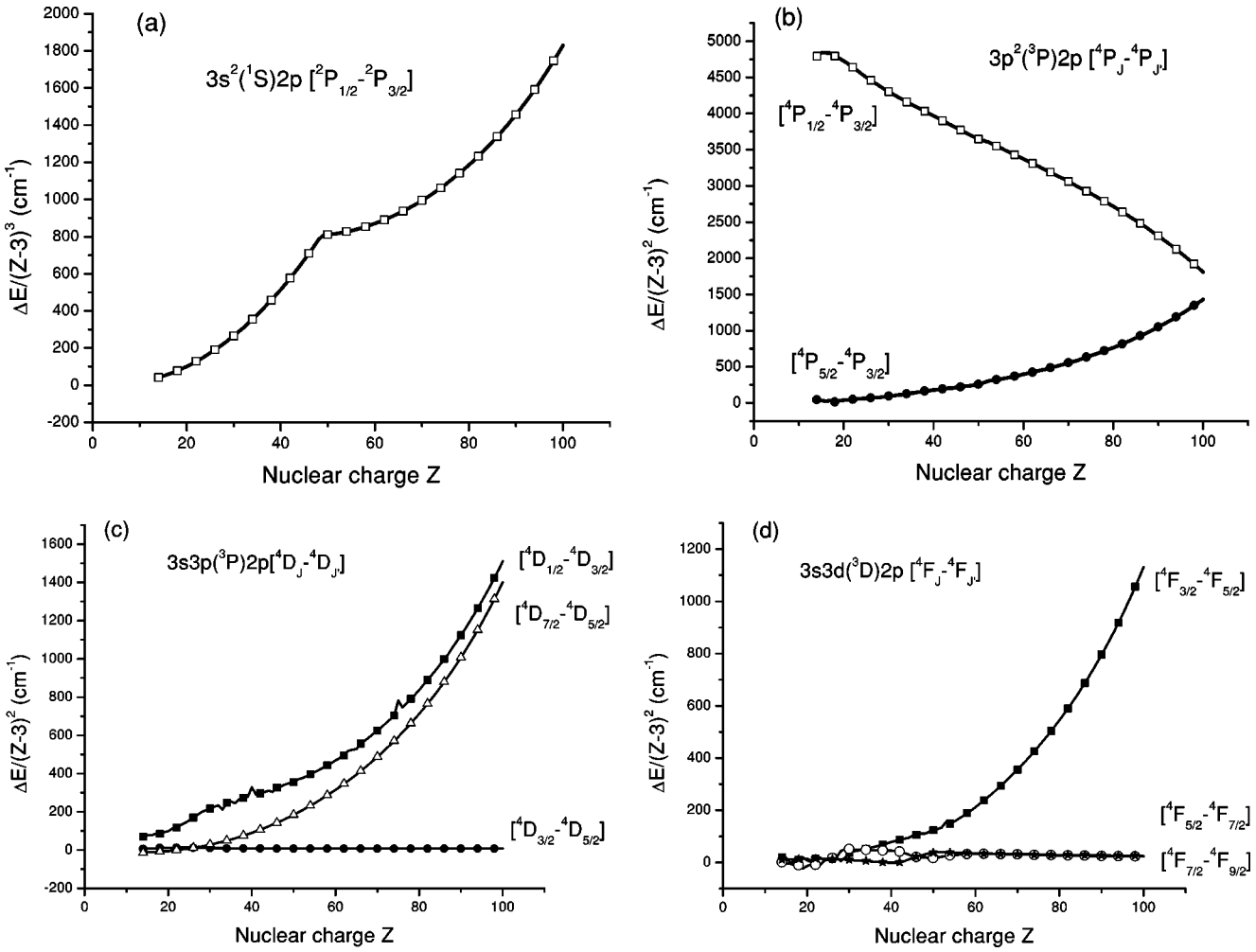

FIG. 5. Energy splittings $[\Delta E/(Z-3)^4$ in cm$^{-1}]$ as functions of Z.

within the doublet or quartet states. The intervals are obtained by subtracting the excitation energies of the corresponding levels (see, for example, Auger data in Table IV). These fine structures are quite regular throughout the isoelectronic sequence, as seen from Fig. 5(a). In this figure, we present the fine-structure splitting divided by $(Z-3)^2$ for the doublet term $3s^2(^1S)2p\ ^2P$. The small deviation from smooth line of Fig. 5(a) in the region of $Z=48-49$ is due to the strong mixing in the odd-parity complex with $J=1/2$ as illustrated in Fig. 3(a). The $3s^2(^1S)2p\ ^2P_{3/2}$ level has smaller energy than the $3s^2(^1S)2p\ ^2P_{1/2}$ level in contradiction with Landé interval rules. The same situation occurs for other fine-structure intervals in Figs. 5(b)–(d). The $^4P_{3/2}$ level has the smallest energy among $3p^2(^3P)2p\ ^4P_J$ levels, the next level is $^4P_{5/2}$, and the $^4P_{1/2}$ level has the largest energy. The value of $(E_{1/2}-E_{3/2})/(Z-3)^2$ decreases with Z while the value of $(E_{5/2}-E_{3/2})/(Z-3)^2$ increases with Z. As a result, energies of $^4P_{1/2}$ and $^4P_{5/2}$ become almost equal for high Z. The energy difference between the $^4D_{3/2}$ and $^4D_{5/2}$ levels in the $3s3p(^3P)2p\ ^4D_J$ quartet term is very small, as shown in Fig. 5(c). We find that the ^4D_J quartet terms are ordered as follows: $^4D_{1/2}$, $^4D_{7/2}$, $^4D_{3/2}$, and $^4D_{5/2}$. Energy differences between the $^4F_{5/2}$, $^4F_{7/2}$, and $^4F_{9/2}$ levels in the $3s3d(^3D)2p\ ^4F_J$ quartet term are very small, as shown in Fig. 5(d). The unusual splitting is caused by the mixing of states within the complexes with different J. Further experimental confirmation would be very helpful in verifying the correctness of these occasionally sensitive mixing parameters.

IV. CONCLUSION

A systematic second-order RMBPT study of the energies of the core-excited states of Na-like ions has been presented. RMBPT gives results in good agreement with experimental and predicted data. It would be beneficial if experimental data for other highly charged Na-like ions were available. At the present time, there are almost no experimental data between $Z=47$ and $Z=100$ for the sodium isoelectronic sequence. Availability of such data could lead to an improved understanding of the relative importance of different contributions to the energies of highly charged ions. These calculations are presented as a theoretical benchmark for comparison with experiment and theory. The present calculations could be further improved by including third-order correlation corrections.

ACKNOWLEDGMENTS

The work of W.R.J. and M.S.S. was supported in part by National Science Foundation Grant No. PHY-01-39928. U.I.S. acknowledges partial support by Grant No. B516165 from Lawrence Livermore National Laboratory. The work of J.R.A was performed under the auspices of the U.S. Department of Energy by the University of California, Lawrence Livermore National Laboratory under Contract No. W-7405-Eng-48.

APPENDIX: THE PARTICLE-PARTICLE-HOLE DIAGRAM

The model space state vector for an ion with two valence electrons (v,w) and one hole (a) can be represented as [23]

$$\Psi(QJM)=N(Q)\sum \langle vw|K_{12}\rangle\langle K_{12}a|K\rangle a_v^\dagger a_w^\dagger a_a|0\rangle, \tag{A1}$$

where $|0\rangle$ is the state vector for the core ($1s^22s^22p^6$ in our case), Q describes a particle-particle-hole state with quantum numbers $n_v^0\kappa_v^0 n_w^0\kappa_w^0 n_a^0\kappa_a^0$, and intermediate momentum J_{12}. We use the notation $K_i=\{J_i,M_i\}$ and $v=\{j_v,m_v\}$. The sum in Eq. (A1) is over magnetic quantum numbers m_v, m_w, m_a, and M_{12}. The quantity $\langle K_1K_2|K_3\rangle$ is a Clebsch-Gordan coefficient,

$$\langle K_1K_2|K_3\rangle=(-1)^{J_1-J_2+M_3}\sqrt{2J_3+1}\begin{pmatrix} J_1 & J_2 & J_3 \\ M_1 & M_2 & -M_3 \end{pmatrix}. \tag{A2}$$

The above representation of the state vector is somewhat inconvenient; for example, it leads to an expression containing 36 terms for the second-order diagram with six free ends. It was shown in Ref. [23] that it is more efficient to express the state vector in a manifestly symmetric form in the case of a three-electron system. Here, we can only use symmetry of two particles v and w. As a result, we obtain the expression for the particle-particle-hole contribution $E_3^{(2)}$ in second order consisting of a sum of E_a, E_b, E_c, and E_d terms:

$$E_3^{(2)}=E_a+E_b+E_c+E_d,$$

$$E_a(v^0w^0[J_{12}]aJ,x^0y^0[J_{13}]bJ)=-\sum_{vw}\sum_{v'w'}P_{J_{12}}(v^0v,w^0w)P_{J_{12}}(x^0v',y^0w')(vw|K_{12})(K_{12}a|K)(v'w'|K_{13})$$
$$\times(K_{13}b|K)\sum_n\frac{g(vwan)g(nbv'w')}{\varepsilon(v)+\varepsilon(w)-\varepsilon(a)-\varepsilon(n)}, \tag{A3}$$

$$E_b(v^0w^0[J_{12}]aJ,x^0y^0[J_{13}]bJ)=\sum_{vw}\sum_{v'w'}P_{J_{12}}(v^0v,w^0w)P_{J_{12}}(x^0v',y^0w')(vw|K_{12})(K_{12}a|K)(v'w'|K_{13})$$
$$\times(K_{13}b|K)\sum_n\left[\frac{g(vww'n)g(nbv'a)-g(vww'n)g(nbav')}{\varepsilon(v)+\varepsilon(w)-\varepsilon(w')-\varepsilon(n)}\right], \tag{A4}$$

$$E_c(v^0w^0[J_{12}]aJ,x^0y^0[J_{13}]bJ)=\sum_{vw}\sum_{v'w'}P_{J_{12}}(v^0v,w^0w)P_{J_{13}}(x^0v',y^0w')(vw|K_{12})(K_{12}a|K)(v'w'|K_{13})$$
$$\times(K_{13}b|K)\sum_n\left[\frac{g(vban)g(nwv'w')-g(bvan)g(nwv'w')}{\varepsilon(v)+\varepsilon(b)-\varepsilon(a)-\varepsilon(n)}\right], \tag{A5}$$

$$E_d(v^0w^0[J_{12}]aJ,x^0y^0[J_{13}]bJ)=\sum_{vw}\sum_{v'w'}P_{J_{12}}(v^0v,w^0w)P_{J_{12}}(x^0v',y^0w')=(vw|K_{12})(K_{12}a|K)(v'w'|K_{13})$$
$$\times(K_{13}b|K)\sum_n\frac{1}{\varepsilon(w)+\varepsilon(b)-\varepsilon(v')-\varepsilon(n)}[-g(wbv'n)g(nvw'a)+g(bwv'n)g(nvw'a)$$
$$+g(wbv'n)g(nvaw')-g(bwv'n)g(nvaw')]. \tag{A6}$$

The quantity $P_J(v^0v,w^0w)$ is a symmetry coefficient defined by

$$P_J(v^0v,w^0w)=\eta_{v^0w^0}[\,\delta_{v^0v}\delta_{w^0w}+(-1)^{j_v+j_w+J+1}\delta_{v^0w}\delta_{w^0v}], \quad \text{(A7)}$$

where η_{vw} is a normalization factor given by

$$\eta_{vw}=\begin{cases} 1 & \text{for } w\neq v \\ 1/\sqrt{2} & \text{for } w=v \end{cases},$$

and $\varepsilon(i)$ is the one-body DF energy of the state i. The quantities $(vw|K_{12})$ are Clebsch-Gordan coefficients and $(K_{12}a|K)$ differs from the definition (A2) by the $(-1)^{j_a-m_a}$ factor and $-m_a$ in the $3j$ coefficient. The indices v, w, x, and y distinguish the valence states; indices a and b refer to the core states; and index n refers to excited states. The two-particle matrix element $g(1234)$ is the sum of the two-particle Coulomb and Breit matrix elements and is presented as a product of radial and angular parts,

$$g(1234)=\sum_k\,(X_k(1234)+B_k(1234))(-1)^{j_1+j_2+m_1+m_2+k}\times\sum_m\,(-1)^m\begin{pmatrix} j_1 & j_3 & k \\ m_1 & -m_3 & m\end{pmatrix}\times\begin{pmatrix} j_2 & j_4 & k \\ m_2 & -m_4 & -m\end{pmatrix}. \quad \text{(A8)}$$

Radial part $X_k(abcd)$ of the Coulomb matrix element is given by

$$X_k(abcd)=(-1)^k(a\|C_k\|c)\langle b\|C_k\|d\rangle R_k(abcd). \quad \text{(A9)}$$

The quantities C_k are normalized spherical harmonics and $R_k(abcd)$ are Slater integrals. The expression for the Breit matrix elements $B_k(1234)$ is given in Ref. [28]. Carrying out angular reduction, we obtain the final expression for the four contributions E_a, E_b, E_c, and E_d to the second-order diagram of particle-particle-hole interaction,

$$E_a(v^0w^0[J_{12}]aJ,x^0y^0[J_{13}]bJ)=\sum_{vw}\sum_{v'w'}P_{J_{12}}(v^0v,w^0w)P_{J_{13}}(x^0v',y^0w')\frac{\sqrt{[J_{12}][J_{13}]}}{[J]}(-1)^{J_{12}+J_{13}}\times\sum_n\sum_k\sum_{k'}\frac{X_k(vwan)X_{k'}(v'w'bn)}{\varepsilon(v)+\varepsilon(w)-\varepsilon(a)-\varepsilon(n)}\delta(J,j_n)\begin{Bmatrix} J_{12} & j_a & j_n \\ k & j_w & j_v\end{Bmatrix}\begin{Bmatrix} J_{13} & j_b & j_n \\ k' & j_{w'} & j_{v'}\end{Bmatrix}\times(-1)^{j_a+j_b+j_{w'}+j_w+k+k'}, \quad \text{(A10)}$$

$$E_b(v^0w^0[J_{12}]aJ,x^0y^0[J_{13}]bJ)=\sum_{vw}\sum_{v'w'}P_{J_{12}}(v^0v,w^0w)P_{J_{13}}(x^0v',y^0w')\sqrt{[J_{12}][J_{13}]}\times\sum_n\sum_k\sum_{k'}\frac{X_{k'}(vww'n)}{\varepsilon(v)+\varepsilon(w)-\varepsilon(w')-\varepsilon(n)}\begin{Bmatrix} j_{w'} & j_n & J_{12} \\ j_w & j_v & k'\end{Bmatrix}(-1)^{1+k+k'}\Bigg[X_k(nbav')\times\begin{Bmatrix} j_b & j_{v'} & k \\ j_{w'} & J & J_{13}\end{Bmatrix}\begin{Bmatrix} j_a & j_n & k \\ j_{w'} & J & J_{12}\end{Bmatrix}(-1)^{J_{12}+J_{13}+j_n+j_{v'}+j_n+j_w}+X_k(nbv'a)\begin{Bmatrix} j_b & j_a & k \\ J_{12} & J_{13} & J\end{Bmatrix}\times\begin{Bmatrix} j_n & j_{v'} & k \\ J_{13} & J_{12} & j_{w'}\end{Bmatrix}(-1)^{j_b+j_{w'}+j_w-J}\Bigg], \quad \text{(A11)}$$

$$E_c(v^0w^0[J_{12}]aJ,x^0y^0[J_{13}]bJ)=\sum_{vw}\sum_{v'w'}P_{J_{12}}(v^0v,w^0w)P_{J_{13}}(x^0v',y^0w')\sqrt{[J_{12}][J_{13}]}\times\sum_n\sum_k\sum_{k'}\frac{X_{k'}(v'w'vn)}{\varepsilon(v')+\varepsilon(w')-\varepsilon(v)-\varepsilon(n)}\begin{Bmatrix} j_v & j_n & J_{13} \\ j_{w'} & j_{v'} & k'\end{Bmatrix}(-1)^{1+k+k'}\Bigg[X_k(wban)\times\begin{Bmatrix} j_a & j_w & k \\ j_v & J & J_{12}\end{Bmatrix}\begin{Bmatrix} j_b & j_n & k \\ j_v & J & J_{13}\end{Bmatrix}(-1)^{J_{13}+j_a+j_{w'}+j_w+j_v}+X_k(bwan)\begin{Bmatrix} j_b & j_a & k \\ J_{12} & J_{13} & J\end{Bmatrix}\times\begin{Bmatrix} j_n & j_w & k \\ J_{12} & J_{13} & j_v\end{Bmatrix}(-1)^{j_b+j_{w'}+j_n+J+J_{12}}\Bigg], \quad \text{(A12)}$$

$$E_d(v^0w^0[J_{12}]aJ,x^0y^0[J_{13}]bJ)=\sum_{vw}\sum_{v'w'}P_{J_{12}}(v^0v,w^0w)P_{J_{13}}(x^0,v',y^0w')\sqrt{[J_{12}][J_{13}]}$$

$$\times\sum_{n}\sum_{kk'}\frac{1}{\varepsilon(w)+\varepsilon(b)-\varepsilon(v')-\varepsilon(n)}(-1)^{1+j_n+j_w+j_a+j_{v'}+J_{12}+J_{13}}$$

$$\times\Bigg[X_k(nvw'a)X_{k'}(bwv'n)\begin{Bmatrix}j_a & j_v & k\\ j_w & J & J_{12}\end{Bmatrix}\begin{Bmatrix}j_b & j_{v'} & k'\\ j_{w'} & J & J_{13}\end{Bmatrix}\begin{Bmatrix}j_w & j_n & k'\\ j_{w'} & J & k\end{Bmatrix}$$

$$+X_k(nvw'a)X_{k'}(wbv'n)\begin{Bmatrix}j_a & j_v & k\\ j_w & J & J_{12}\end{Bmatrix}\sum_{\kappa}[\kappa]\begin{Bmatrix}j_b & j_{v'} & \kappa\\ j_{w'} & J & J_{13}\end{Bmatrix}\begin{Bmatrix}j_w & j_n & \kappa\\ j_{w'} & J & k\end{Bmatrix}$$

$$\times\begin{Bmatrix}j_b & j_{v'} & \kappa\\ j_w & j_n & k'\end{Bmatrix}+X_k(nvaw')X_{k'}(bwv'n)\begin{Bmatrix}j_b & j_{v'} & k'\\ j_{w'} & J & J_{13}\end{Bmatrix}\sum_{\kappa}[\kappa]\begin{Bmatrix}j_a & j_v & \kappa\\ j_w & J & J_{12}\end{Bmatrix}$$

$$\times\begin{Bmatrix}j_{w'} & j_n & \kappa\\ j_w & J & k'\end{Bmatrix}\begin{Bmatrix}j_a & j_v & \kappa\\ j_{w'} & j_n & k\end{Bmatrix}+X_k(nvaw')X_{k'}(wbv'n)\begin{Bmatrix}j_a & j_v & k\\ j_w & J & J_{12}\end{Bmatrix}$$

$$\times\begin{Bmatrix}j_b & j_{v'} & k'\\ j_{w'} & J & J_{13}\end{Bmatrix}\sum_{\kappa\kappa'}[\kappa][\kappa']\begin{Bmatrix}j_a & j_v & \kappa\\ j_{w'} & j_n & k\end{Bmatrix}\begin{Bmatrix}j_b & j_{v'} & \kappa'\\ j_w & j_n & k'\end{Bmatrix}\begin{Bmatrix}j_w & j_n & \kappa'\\ j_{w'} & J & \kappa\end{Bmatrix}\Bigg]. \quad \text{(A13)}$$

[1] H. L. Zhang, D. H. Sampson, R. E. H. Clark, and J. B. Mann, At. Data Nucl. Data Tables **41**, 1 (1989).

[2] R. D. Cowan, *The Theory of Atomic Structure and Spectra* (University of California Press, Berkeley, 1981).

[3] M. H. Chen, Phys. Rev. A **40**, 2365 (1989).

[4] J. Nilsen, At. Data Nucl. Data Tables **41**, 131 (1989).

[5] R. Bruch, U. I. Safronova, A. S. Shlyaptseva, J. Nilsen, and D. Schneider, Phys. Scr. **57**, 334 (1998).

[6] R. Bruch, U. I. Safronova, A. S. Shlyaptseva, J. Nilsen, and D. Schneider, J. Quant. Spectrosc. Radiat. Transf. **69**, 605 (1998).

[7] M. A. Bautista, J. Phys. B **33**, 71 (2000).

[8] W. Eissner, M. Jones, and H. Nussbaumer, Comput. Phys. Commun. **8**, 270 (1974).

[9] J. Sugar and C. Corliss, J. Phys. Chem. Ref. Data Suppl. **2**, 100 (1985).

[10] T. Shirai, Y. Funatake, K. Mori, J. Sugar, W. L. Wiese, and Y. Nakai, J. Phys. Chem. Ref. Data **19**, 127 (1990).

[11] P. G. Burkhalter, L. Cohen, R. D. Cowan, and U. Feldman, J. Opt. Soc. Am. **69**, 1133 (1979).

[12] C. Jupén, L. Engstrom, R. Hutton, and E. Träabert, J. Phys. B **21**, L347 (1988).

[13] D. Schneider, M. H. Chen, S. Chantrenne, R. Hutton, and M. H. Prior, Phys. Rev. A **40**, 4313 (1989).

[14] R. Hutton, D. Schneider, and M. H. Prior, Phys. Rev. A **44**, 243 (1991).

[15] S. Bliman, R. Bruch, P. L. Altick, D. Schneider, and M. H. Prior, Phys. Rev. A **53**, 4176 (1996).

[16] K. J. H. Phillips, C. J. Greer, A. K. Bhatia, I. H. Coffey, R. Barnsley, and F. P. Keenan, Astron. Astrophys. **324**, 381 (1997).

[17] G. V. Brown, P. Beiersdorfer, M. Chen, M. H. Chen, and K. Reed, Astrophys. J. **557**, L75 (2001).

[18] S. A. Blundell, Phys. Rev. A **47**, 1790 (1993).

[19] U. I. Safronova, W. R. Johnson, and H. G. Berry, Phys. Rev. A **61**, 052503 (2000).

[20] U. I. Safronova, C. Namba, I. Murakami, W. R. Johnson, and M. S. Safronova, Phys. Rev. A **64**, 012507 (2001).

[21] P. Beiersdorfer, M. Bitter, S. von Goeler, S. Cohen, K. W. Hill, J. Timberlake, R. S. Walling, M. H. Chen, P. L. Hagelstein, and J. H. Scofield, Phys. Rev. A **34**, 1297 (1986).

[22] P. Beiersdorfer, J. Nilsen, J. H. Scofield, M. Bitter, S. von Goeler, and K. W. Hill, Phys. Scr. **51**, 322 (1995).

[23] M. S. Safronova, W. R. Johnson, and U. I. Safronova, Phys. Rev. A **54**, 2850 (1996).

[24] U. I. Safronova, W. R. Johnson, and M. S. Safronova, At. Data Nucl. Data Tables **69**, 183 (1998).

[25] U. I. Safronova, C. Namba, J. R. Albritton, W. R. Johnson, and M. S. Safronova, Phys. Rev. A **65**, 022507 (2002).

[26] M. S. Safronova, W. R. Johnson, and U. I. Safronova, J. Phys. B **30**, 2375 (1997).

[27] L. D. Landau and E. M. Lifshitz, *Quantum Mechanics-Non-Relativistic Theory* (Pergamon Press, London, 1963).

[28] W. R. Johnson, S. A. Blundell, and J. Sapirstein, Phys. Rev. A **37**, 2764 (1988).